Journal of Statistical Physics, Vol. 81, Nos. 1/2, 1995

Phase Separation in a Three-Dimensional, Two-Phase, Hydrodynamic Lattice Gas

Cécile Appert,[1] John F. Olson,[2] Daniel H. Rothman,[2] and Stéphane Zaleski[3]

Received December 5, 1994; final May 2, 1995

The dynamics of phase separation is explored using an immiscible 3D lattice-gas model. Scaling laws for the growth rate and power spectra $S(k)$ of the growth patterns are computed. For small wavenumbers $S(k)$ shows a crossover from k^2 to k^4 behavior. The theoretical prediction for the asymptotic domain growth $R \simeq t^{2/3}$ is supported by our results. We discuss the possibility to observe an intermediate t scaling. We show the influence of hydrodynamic forces in symmetric and asymmetric mixtures by comparing simulations with and without momentum conservation. The structure function $S(k)$ is not significantly modified by hydrodynamics, but the growth rate changes clearly. As a general result, it is shown that, in spite of the unusual thermodynamics of this model, many characteristics of the growth dynamics are surprisingly in agreement with the classical theoretical and experimental results.

KEY WORDS: Lattice-gas automata; immiscible fluids; phase separation; spinodal decomposition, growth dynamics.

1. INTRODUCTION

Different mechanisms in binary mixtures may lead to phase separation. They are classified according to the nature of the initial destabilizing perturbation. Nucleation requires that the amplitude of the perturbation

[1] Laboratoire de Physique Statistique, École Normale Supérieure, CNRS, Paris Cedex 05, France. E-mail: appert@physique.ens.fr.

[2] Department of Earth, Atmospheric and Planetary Sciences, MIT, Cambridge, Massachusetts 02139. E-mail: john@segovia.mit.edu; dan@segovia.mit.edu.

[3] Laboratoire de Modélisation en Mécanique, CNRS, Université Pierre et Marie Curie, 75252 Paris Cedex 05, France. E-mail: zaleski@lmm.jussieu.fr.

0022-4715/95/1000-0181$07.50/0

should be larger than a certain threshold, whereas in spinodal decomposition an infinitesimal perturbation of a sufficient wavelength will lead to phase separation.[1,2]

Spinodal decomposition has elicited great interest during the past decades, in part because the mechanical properties of an alloy depend on the dynamics of the phase separation process. Spinodal decomposition may also involve only fluids. Examples of fluid–fluid phase separation include the liquid–gas phase transition and the separation of two immiscible fluids. In this case the effects of hydrodynamics must be taken into account to fully characterize the process.

One way to describe phase separation is via the evolution of an order parameter (which may be, for example, the local density or the local concentration of a chemical species), as in the Cahn–Hilliard equation.[3,4] An efficient numerical method for this equation is the cell-dynamical systems method.[3] However, it is difficult to incorporate hydrodynamic effects in this approach, although efforts have been made in this direction.[3,7,6]

An alternative way to account for hydrodynamics is to solve the full Navier–Stokes equations in the presence of interfaces. This is possible with lattice-gas automata (LGA) or related lattice-Boltzmann methods. These methods are based on kinetic fluid models which may undergo spontaneous spinodal decomposition. Surface tension arises spontaneously from the evolution rules leading to phase separation.[8]

In this paper we apply a Boolean lattice gas to the study of the dynamics of phase separation. We use a 3D version[9] of the 2D immiscible lattice gas (ILG).[10] Note that connectivity properties of domains and thus dynamics of phase separation are different in two and three dimensions.

A characteristic feature of LGA is that, due to the Boolean nature of the variables, which cannot account for infinitesimal variations, microscopic noise stems directly from the evolution rules. Here, as we are interested in averaged quantities, the presence of noise does not perturb the results. Besides, as noise is automatically coupled with hydrodynamics, it allows simulation of the important role of fluctuations in phase separation.

Phase separation may alternatively be studied with related Boltzmann methods.[11–13] In this case noise must be added explicitly. For example Chen and Lookman[13] perturb the interface orientation at each time step. It may be interesting to compare the results obtained from these methods with Boolean simulations to gain some insight on how noise affects the dynamics of phase separation.

The paper is organized as follows. We first recall the definition of the 3D ILG model and then present our results from simulations. Section 3.1 discusses the shape of the power spectrum of the growth patterns. After some introductory definitions and remarks on finite-size effects (Sections

3.2.1 and 3.2.2), the growth dynamics is studied in Section 3.2.3. In Section 3.3, we study a variant of our model in which momentum conservation is broken. Comparison with simulations of the momentum-conserving model shows the contribution of hydrodynamic forces to phase separation.

2. DEFINITION OF THE 3D ILG MODEL

The 3D ILG model[9] has been built on top of the now classical FCHC lattice gas.[14] At each time step, pointlike particles hop from site to site on a lattice and collide when they meet at a site according to predefined rules which conserve mass and momentum. Particle velocities $\{\mathbf{c}_i\}_{i=1,\ldots,24}$ can take only a finite number of values, corresponding to the directions of the lattice. An exclusion principle ensures that no more than one particle will have a given velocity at a given site, and thus the configuration at one site can be represented as a Boolean vector.

In the ILG model there are two species of particles, red and blue. The Boolean variables $r_i(\mathbf{x})$ and $b_i(\mathbf{x})$ indicate the presence of a red or blue particle with velocity $\mathbf{c}_i$ at site $\mathbf{x}$. Particles with the same color attract each other, whereas particles with different colors repel each other.[10] Because the interaction rules of the 3D ILG are somewhat different from the 2D model, we recall them briefly below.

In the first step of the 3D ILG dynamics, colorblind (i.e., classical FCHC) collisions are performed. The result is then modified in order to create surface tension. To perform this modification, the interface orientation is first evaluated through the measurement of the color gradient

$$\mathbf{f} = \sum_i \mathbf{c}_i [\rho_R(\mathbf{x}+\mathbf{c}_i) - \rho_B(\mathbf{x}+\mathbf{c}_i)] \tag{1}$$

where ρ_R and ρ_B are the total number of red and blue particles in a given site, respectively. We then choose pairs of particles with opposite velocities and try to align them parallel to the color gradient. This operation is performed only if the modulus of $\mathbf{f}$ is greater than a given threshold, that is, only on the interface.

Second, colors are redistributed among velocity states. The selected configuration is the one which maximizes the scalar product $\mathbf{q} \cdot \mathbf{f}$, where $\mathbf{q}$ is the color flux after collision

$$\mathbf{q} = \sum_i [r'_i(\mathbf{x}) - b'_i(\mathbf{x})]\, \mathbf{c}_i \tag{2}$$

where $r'_i(\mathbf{x})$ and $b'_i(\mathbf{x})$ stand for the output values of $r_i(\mathbf{x})$ and $b_i(\mathbf{x})$ after collision. This choice creates a negative diffusion, resulting for a range of parameters in a spontaneous separation of the two fluids.

Lastly, in the propagation step, more particles move in the direction normal to the interface than in the tangential direction. Surface tension results[9] due to anisotropy of pressure on the interface, as can be seen from its mechanical definition,

$$\sigma = \int_{-\infty}^{+\infty} [p_n - p_t(x)]\, dx \tag{3}$$

where x is the coordinate normal to the interface and p_n and p_t are the pressures normal and tangential to the interface, respectively.

3. SIMULATIONS OF PHASE SEPARATION

The lattice is initialized with a homogeneous mixture of red and blue particles, which separate spontaneously during the simulation. The maxi-

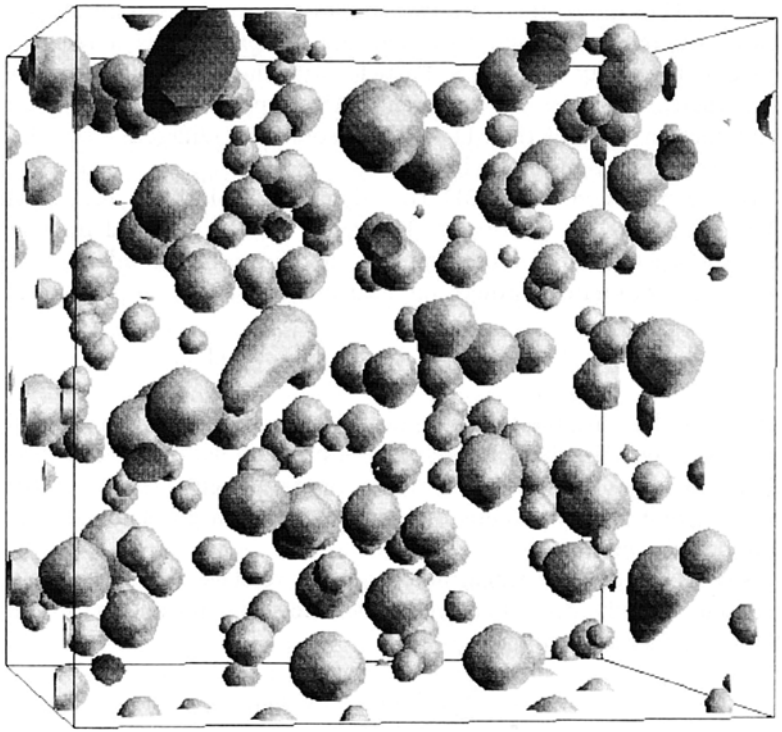

Fig. 1. Phase separation after 6301 time steps, for a volume fraction of red equal to 5%. Only interfaces are shown. The red phase is dispersed in the blue phase in the form of small droplets. Boundary conditions are periodic. The average density is 12 particles per site. The lattice size is 128^3.

Table I. Code Speed for the 3D ILG Model

Computer	Code speed (× 1000 sites per second)
SPARC II	31
HP 730	57
IBM RS 6000-370	109

mal lattice size that we have simulated is 128^3. Time performances of the code are summarized in Table I. A typical 128^3 simulation on a HP 730 workstation takes about 4 days for 10,000 time steps.

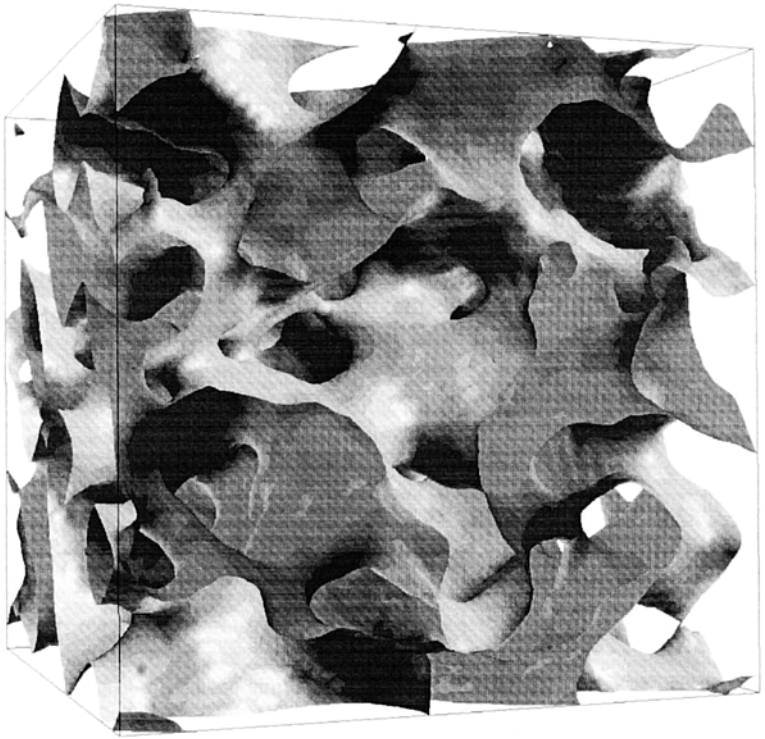

Fig. 2. Spinodal decomposition after 3032 time steps, for a volume fraction of red equal to 50%. Only interfaces are shown. Both phases are continuously interconnected. Boundary conditions are periodic. The average density is 12 particles per site. The lattice size is 128^3.

An important parameter is the volume fraction of the red phase, also called the red concentration, defined by

$$\theta = \frac{\rho_R}{\rho_R + \rho_B} \tag{4}$$

Purely blue and red phases correspond respectively to $\theta = 0$ or 1. Figures 1 and 2 show phase separation for $\theta = 5\%$ and 50%. For small volume fractions, red particles gather in separated droplets, whereas for concentrations near 50% both phases are continuously connected; the transition from unconnected to connected phases occurs at volume fractions between 0.2 and 0.35.

3.1. Power Spectrum of the Color Density Field

The power spectrum is measured at different times during simulations. Its definition is[4]

$$S(\mathbf{k}) = \frac{1}{N} \left| \sum_{\mathbf{x}} [\theta(\mathbf{x}) - \bar{\theta}] \exp(i\mathbf{k} \cdot \mathbf{x}) \right|^2 \tag{6}$$

where $\theta(\mathbf{x})$ is the red concentration at site $\mathbf{x}$ and $\bar{\theta}$ is the volume average. The system is assumed to be isotropic and a radial average is performed to obtain $S(k)$, where $k = |\mathbf{k}|$. The evolution of the power spectrum $S(k)$ with time for a mixture with $\theta = 0.5$ is shown in Fig. 3. As time increases, the domains grow and thus the maximum of $S(k)$ moves to the left. The distribution becomes more sharply peaked.

If we assume that the observed patterns are self-similar in time, then $S(k)$ must follow the scaling law

$$S(k) = R^3(t)\, F(kR(t)) \tag{7}$$

where $R(t)$ is a characteristic size of the domains.[2, 3] We discuss the function $R(t)$ in the next section, but in the meantime define the dimensionless wavenumber

$$q = kR(t) \tag{8}$$

[4] Some calculations were performed for a different definition, namely

$$S(\mathbf{k}) = \frac{1}{N} \left| \sum_{\mathbf{x}} [\rho_R - \rho_B] \exp[i\mathbf{k} \cdot \mathbf{x}] \right|^2 \tag{5}$$

As density is almost constant in the ILG model,[15] the above definition is proportional to definition (6) by a factor of $4\rho^2$.

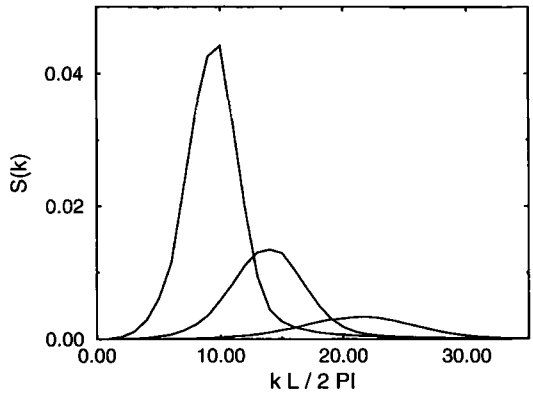

Fig. 3. Power spectrum of the color field at time steps $t = 25$, 113, and 279. The average density is 20 particles per site and the average volume fraction of red is 50%. The size L of the simulation box is 128. As time increases, the domains grow and thus the maximum of $S(k)$ moves to the left. The distribution also becomes more sharply peaked.

Simulations show that the self-similarity assumption is well verified if the early stages of phase separation are excluded, as illustrated by Fig. 4 for an average volume fraction of red $\theta = 0.5$ and by Fig. 5 for $\theta = 0.05$. However, if we use open and solid symbols for early and late times respectively, a slight drift of $F(q)$ with time is found. This is not very surprising, because different physical mechanisms become dominant in the dynamics at different times.

The use of logarithmic axes shows the behavior of $F(q)$ at large and small q. For small wavelengths ($q \gg 1$), $F(q)$ scales as q^{-4}, at least in first approximation. This well-known behavior, called Porod's law, stems from the existence of thin, well-defined interfaces on length scales smaller than the typical radius of curvature.[16, 3] When q is only slightly greater than 1, interfaces at the corresponding scale look entangled. Then next-order terms in the development of $F(q)$ become important and a q^{-6} or higher order behavior is observed, as demonstrated by Tomita.[18] The shoulder separating the two scaling laws has been found both in numerical simulations[19] and laboratory experiments[20] to occur at $q \simeq 3$. Our own observations are in agreement with these results. The arrow located at $q = 3$ in Fig. 4B points to the shoulder. We found that our simulations do not satisfy Tomita's sum rule.[17, 18] This could be explained by the fact that the asymptotic regime has not yet been reached.

An interesting crossover in the scaling of the structure function $F(q)$ occurs for q-values less than 1. For a volume fraction of red equal to

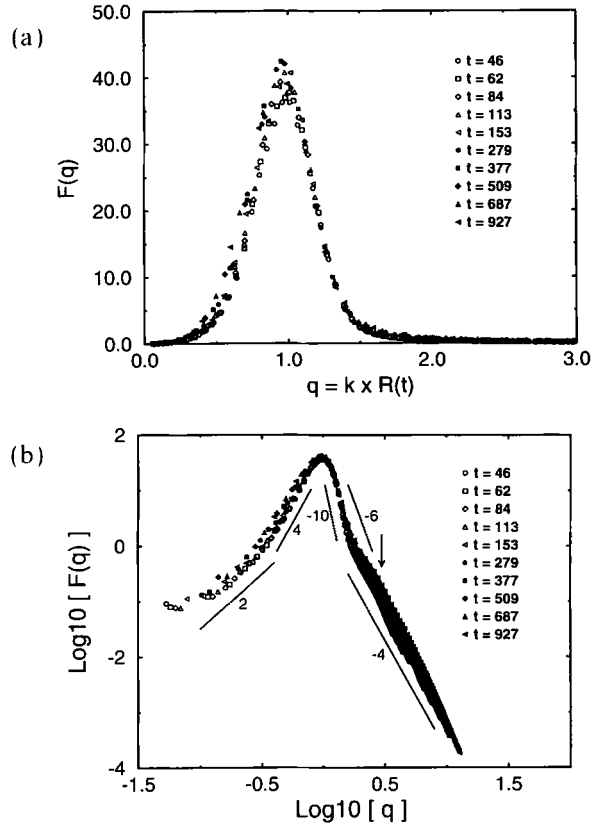

Fig. 4. Check of the scaling law (7) for a volume fraction of red 50% and an average density of 20 particles per site. Natural and logarithmic plots. For $q \gg 1$ we recover the expected Porod law q^{-4}. For $q \gtrsim 1$ the exponent is greater due to the entanglement of interfaces. The arrow on the logarithmic plot indicates the location $q = 3$.

50% our results support a q^4 scaling for $0.3 < q < 1$, which turns into q^2 below 0.3. To interpret this, we shall assume that hydrodynamic forces do not influence significantly the shape of $F(q)$. This will be checked in Section 3.3. Then the theoretical predictions of Yeung[21] and Furukawa[22] for the structure function at small q, which do not take into account hydrodynamics, should apply here.

The method employed by Yeung[21] is the following. From the Cahn–Hilliard–Cook evolution equation (including thermal noise) for the order parameter, a differential equation for $F(q)$ can be found. Some coefficients of this equation depend on time, mainly through $R(t)$, and so $F(q)$ changes with time. Yeung evaluates the order of magnitude of the different terms of

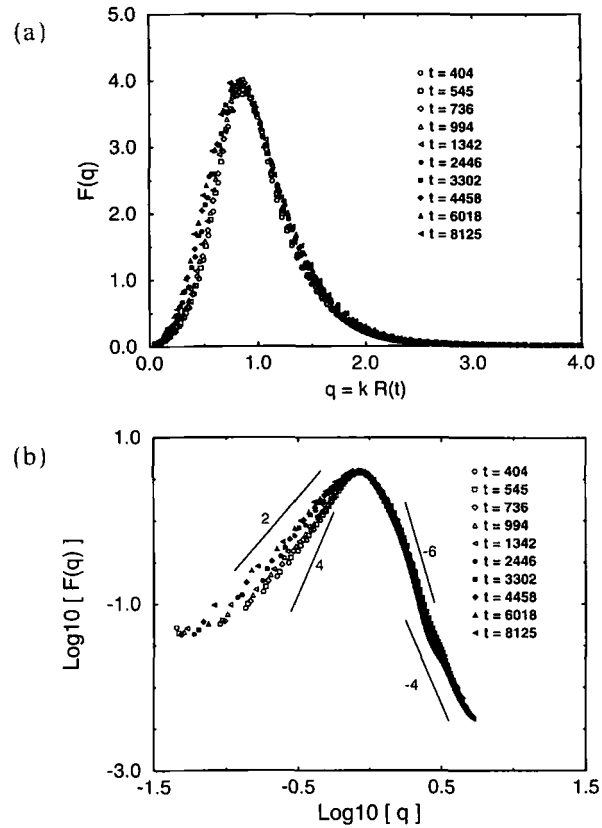

Fig. 5. Check of the scaling law (7) for a volume fraction of red equal to 5% and an average density of 20 particles per site. Natural and logarithmic plots. For $q \gg 1$ we recover the expected Porod law q^{-4}. For $q \gtrsim 1$ the next-order term q^{-6} becomes dominant. The function at small q scales as q^2 rather than q^4.

the equation that determines $F(q)$. He shows that once the asymptotic limit is reached, the definition of $F(q)$ is dominated by a term linked to the choice of the chemical potential and scaling as q^4 at small q. However, in earlier stages another term scaling like $R^{-2}q^2$ due to thermal fluctuations may dominate. This term becomes negligible when $R(t)$ is sufficiently large, that is, for sufficiently late times. It should be noticed, however, that for each $R(t)$ there is a value of q below which the fluctuation term will no longer be negligible.

As we discuss in Section 3.2.2, in our simulations the largest value of $R(t)$ before finite-size effects become significant is only about 25. Then the q^4 term will be dominant over the $R^{-2}q^2$ term only for q greater than 0.4

(we are not accounting for the coefficients of these terms, so this evaluation is only qualitative). Indeed we find a crossover between the q^2 and q^4 behavior at $q \simeq 0.3$, which is the correct order of magnitude.

This crossover points out that we have not reached the asymptotic regime. Indeed it turns out that most numerical results have been obtained for nonasymptotic behaviors. Although Shinozaki and Oono[3] and Koga and Kawasaki[19] reported an observation of q^4 behavior of $F(q)$ in cell dynamical systems simulations, they had no point below $q = 0.3$, making it difficult to conclude to what extent they reached the asymptotic regime. In another case, Alexander *et al.*[12] find only a q^2 behavior in their 3D simulations. However, their results seem to indicate that the asymptotic regime has not been reached and that the slope of $F(q)$ at small q keeps growing with time. Thus the discrepancy that they find with Yeung's prediction is not surprising.

3.2. Domain Growth

3.2.1. Choice of a Definition for the Characteristic Domain Size. From the power spectrum of the color field, several characteristic sizes may be extracted. The simplest one comes from the first moment:

$$R(t) = \frac{\int S(k)\, dk}{\int kS(k)\, dk} \tag{9}$$

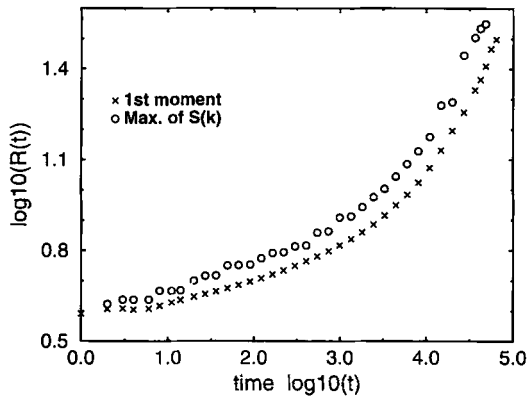

Fig. 6. Comparison of two definitions of the characteristic size $R(t)$, based respectively on the first moment of $S(k)$ (crosses) and its maximum (circles). The volume fraction of red is 5%. The average density is 20 particles per site. The evolution for both quantities is similar. No simple power law is evident.

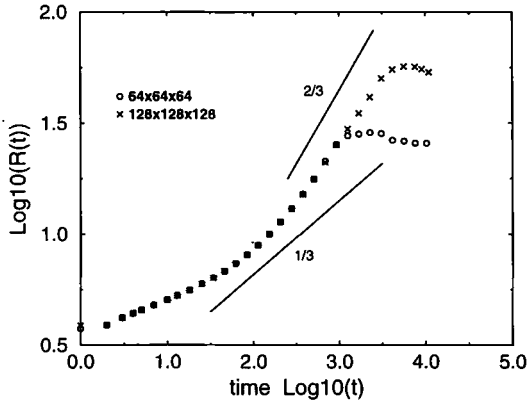

Fig. 7. Characteristic size for 64^3 and 128^3 boxes, for a volume fraction of red $\theta = 0.5$. The average density is 20 particles per site. Before time $t = 927$, both curves merge and finite-size effects are thus proved to be negligible. The effective growth is more rapid than $t^{1/3}$ because of hydrodynamic effects. Our results are compatible with an asymptotic 2/3 exponent.

Another possible definition is the size corresponding to the maximum of the spectrum $S(k)$. In this case we use a parabolic fit of the maximum and its nearest neighbors.

The time evolution of the characteristic size has been measured in simulations. Results do not depend significantly on the choice for the definition of $R(t)$ (see Fig. 6). However, the definition based on the maximum of $S(k)$ gives noisier measurements. Thus in what follows we use the first moment as defined by Eq. (9).

3.2.2 Finite-Size Effects. It is also necessary to know when the phase separation will become sensitive to the finite size of the box. We have compared results of simulations on lattices of different sizes. If the results were independent of the size of the lattice, we would expect that they would be identical for all lattices of sufficient size. Indeed Fig. 7 shows that for a volume fraction of red $\theta = 0.5$ the measurements in 64^3 and 128^3 boxes give the same characteristic size $R(t)$ until time $t \simeq 1000$. Another method is to check, using power spectra, the time up to which the assumption of self-similarity is valid. Both methods give similar estimates for the time beyond which finite-size effects become sensitive.

The comparison of independent simulations in Figure 7 also yields an estimate of the error in $R(t)$, which is much smaller than the symbols on the graph when measurements are based on the first moment of $S(k)$.

3.2.3. Growth Exponents. The evolution of the characteristic size is related to the nature of the physical phenomena driving the decom-

position. It is usual to look for a growth law in the form t^{α}. Lifshitz and Slyozov[23] predicted an exponent 1/3 when the growth is due to evaporation or condensation on given sections of the interface, with material diffusion between the interfaces. This mechanism is dominant after a transient for systems without hydrodynamics such as binary alloys. The exponent α does not depend on space dimension. However, the observation of an exponent 1/3 at intermediate or late times may also be explained by the Brownian motion of droplets and their coalescence.[24]

For fluid systems, another mechanism described by Siggia[24] becomes dominant at intermediate times if both phases are sufficiently connected. This will be true in particular for $\theta = 50\%$. Surface tension effects are then balanced by viscous forces. The predicted exponent α is 1, as may be found from a dimensional analysis applied to $\nabla(p/\rho) = \nu\nabla^2 v$. Indeed, if $R_1(t)$ is the typical length scale of the domains in this regime (it is assumed that there is only one length scale R_1), then the dimensional analysis yields that R_1 is proportional to $(\sigma/\eta)t$, where η is the dynamical viscosity $\eta = \rho\nu$.[24]

This regime may be followed by an exponent 2/3 when inertial effects become dominant over viscous effects.[16] We call then $R_2(t)$ the typical length scale. The dimensional analysis applied to $\nabla(p/\rho) = v\nabla v$ yields $R_2(t)$ proportional to $(\sigma/\rho)^{1/3}t^{2/3}$.

Figure 7 allows comparison of our results with these different predictions. Clearly the growth exponent becomes greater than 1/3, which can be explained by hydrodynamic interactions. As a result of the size limitation, we were not able to fully reach the asymptotic regime of $t^{2/3}$ growth. However, our results seem to support this asymptotic value for the exponent. As we will discuss now, it is not obvious that we should observe the intermediate-t regime.

The crossover between the two regimes t and $t^{2/3}$ occurs after a time t_c proportional to $\eta^3/(\rho\sigma^2)$, as obtained from $R_1(t_c) = R_2(t_c)$. Then the typical size is

$$R_c \simeq \frac{\eta^2}{\rho\sigma} \tag{10}$$

Notice that the crossover takes place when the Reynolds number $R_e \simeq R_i^2(t)/(\nu t)$ (which increases with time in both cases $i = 1$ or 2) becomes of the order of one.

For a water/air mixture, the scale R_c is of the order of $10^{-2}\,\mu$m. For most other fluid mixtures, it is much larger. That is why the t regime is commonly observed in real experiments. However lattice gas models, including ours, are usually designed to have small η and large σ, in order to reach rapidly macroscopic sizes. Thus R_c may be too small in our case

to allow an observation of the t regime. Indeed, for $\rho = 20$, we obtain $\sigma = 0.689 \pm 0.007$ (lattice units) from the Laplace law and $\nu = 0.107 \pm 0.001$ from the decay of shear waves. Thus R_c would be of the order of 1! It is worth noticing that this effect only depends on the values of the parameters, and not on deeper properties of the model, such as the dynamical nature of the phase transition, or the absence of interaction potential.

3.3. Hydrodynamic Influence

In order to highlight the influence of hydrodynamic forces in the growth dynamics, we have performed some simulations in which momentum conservation is intentionally broken. For 10% of collisions, we reverse the particle velocities as on a solid site.

First we compare the evolution of the characteristic size $R(t)$ with and without momentum conservation. For a 50% mixture, when momentum is not conserved, we recover an exponent 1/3 (Fig. 8) corresponding to the coalescence mechanism. If we double the rate of velocity reversal, we find the same result.

We performed the same comparison for $\theta = 5\%$ (Fig. 9). The growth is strongly slowed down, and we do not reach the asymptotic regime. We expect the non-momentum-conserving simulation to converge toward a $t^{1/3}$

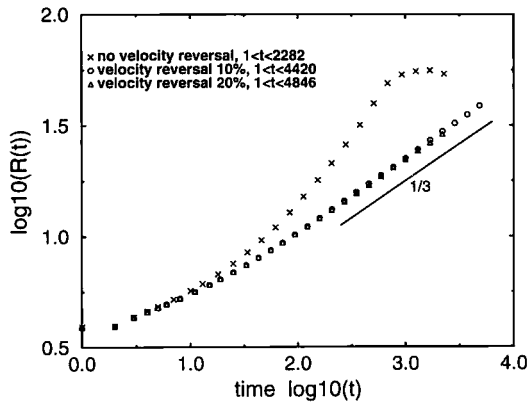

Fig. 8. Growth of the characteristic size as a function of time (logarithmic plot) for $\theta = 0.5$. Simulations with (crosses) and without (circles and triangles) momentum conservation are compared. They were performed with an average density of 12 particles per site. Each result corresponds to only one simulation. For comparison, we have drawn a straight line corresponding to $t^{1/3}$ growth. Only the simulations without momentum conservation follow this growth law.

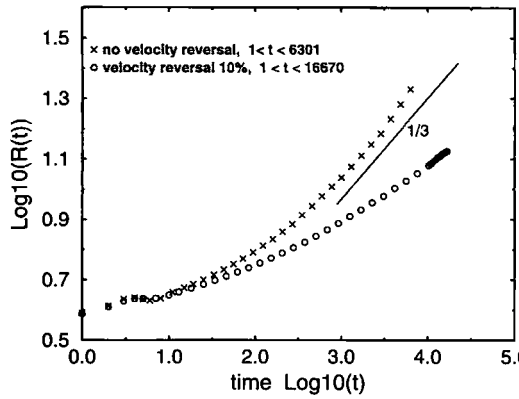

Fig. 9. Growth of the characteristic size as a function of time (logarithmic plot) for $\theta = 0.05$. Simulations with (crosses) and without (circles) momentum conservation are compared. They were performed with an average density of 12 particles per site. The asymptotic regime is apparently not reached in either simulation. However, the momentum-conserving dynamics is more rapid than $t^{1/3}$ in the last time steps, as a consequence of hydrodynamic effects. The dynamics without momentum conservation is much slower, but we expect it to reach a $t^{1/3}$ behavior at large times.

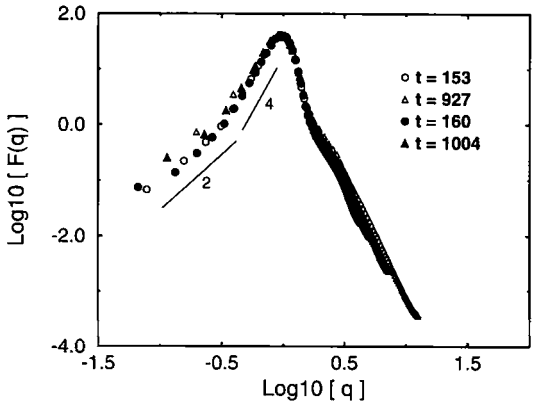

Fig. 10. Comparison of the structure function $F(q)$ with (open symbols) and without (solid symbols) momentum conservation. The volume fraction of red is 50% and the average density is 20 particles per site. No significant difference is introduced by the breaking of momentum conservation.

behavior at late times. We check that for the latest times that have been reached, the growth in the case of a momentum-conserving dynamics is more rapid than $t^{1/3}$. The difference between the two curves makes clear the influence of hydrodynamics on the growth dynamics. We note that Chen and Lookman performed a similar comparison with a Boltzmann method,[13] by resetting the average velocity in each site to zero after the collision step. They also observed a strong slowing down of the dynamics evolving at long times toward a $t^{1/3}$ behavior.

Lastly, Fig. 10 shows the comparison of the structure function $F(q)$ with and without momentum conservation for a volume fraction of red 50%. At first sight, no significant difference is found. This confirms the suggestion of Koga and Kawasaki[19] that $F(q)$ is mostly insensitive to the presence of hydrodynamic interactions, and supports the assumption that allowed us to use the Yeung theory in Section 3.1. A more thorough study of the universality properties of $F(q)$ is, however, beyond the scope of this paper.

4. CONCLUSION

The dynamics of phase separation has been explored using a 3D lattice-gas model for two immiscible fluids. The assumption of domain self-similarity in time is well verified. For large wavenumbers, we recover in first approximation the expected scaling for the structure function $F(q)$, that is, q^{-4} for $q \gg 1$ and $q^{-\gamma}$ with $\gamma \geqslant 6$ for $q \gtrsim 1$. For $q < 1$ it is shown that previous numerical results[3, 19, 12] are not contradictory and can be explained by the fact that the asymptotic regime has not been fully reached. This is illustrated in our case by a crossover from q^2 to q^4 scaling at $q \simeq 0.3$.

Even if the asymptotic regime is not fully reached due to finite-size limitations, our results support an asymptotic $t^{2/3}$ behavior for the growth of domains, in agreement with the theoretical prediction.

We have also intentionally broken momentum conservation in our model in order to demonstrate the contribution of hydrodynamic interactions to the growth dynamics. Without momentum conservation, the domain growth is slowed down and we find the expected $t^{1/3}$ growth for a 50% mixture.

As a general result, we find that spinodal decomposition in lattice gases retains the generic features that have been found from various laboratory experiments, theoretical calculations, and numerical simulations based on a postulated definition for the free energy. This was not obvious

a priori, as no Gibbs free energy can be defined for the model employed here, and the decomposition results only from the dynamical rules. Naively we might have expected that the phase separation characteristics would depend strongly on the thermodynamic properties. On the contrary, in the absence of the usual thermodynamics, the dynamical constraints introduced in our lattice gas model are shown to yield the essential features of the growth dynamics of phase separation.

ACKNOWLEDGMENTS

We thank Dominique d'Humières for suggesting the comparison of simulations with and without momentum conservation. This work was supported in part by NSF grant 9218819-EA7, NATO grant no. 891061, the sponsors of the MIT Porous Flow Project, the Centre National des Etudes Spatiales (CNES), and the donors of the Petroleum Research Fund, administered by the Amercican Chemical Society. Part of this work was performed during a visit of D.R. to the Laboratoire de Physique Statistique supported by the Ecole Normale Supérieure.

REFERENCES

1. F. F. Abraham, On the thermodynamics, structure and phase stability of the nonuniform fluid state, *Phys. Rep.* **53**:93–156 (1979).
2. J. D. Gunton, M. San Miguel, and Paramdeep S. Sahni, The dynamics of first-order phase transitions, in *Phase Transitions and Critical Phenomena*, Vol. 8, C. Domb and J. L. Lebowitz, eds. (Academic Press, New York, 1983), pp. 266–482.
3. A. Shinozaki and Y. Oono, Spinodal decomposition in 3D-space, *Phys. Rep.* **48**:2622–2654 (1993).
4. J. W. Cahn and J. E. Hilliard, Free energy of a nonuniform system. I. Interfacial free energy, *J. Chem. Phys.* **28**:258–267 (1958).
5 A. J. Bray, Exact renormalization-group results for domain-growth scaling in spinodal decomposition, *Phys. Rev. Lett.* **62**:2841 (1989).
6. O. T. Valls and J. E. Farrell, Spinodal decomposition in a three-dimensional fluid model, *Phys. Rep.* **47**:R36 (1993).
7. S. Puri and B. Dünweg, Temporally linear domain growth in the segregation of binary fluids, *Phys. Rev. A* **45**:R6977 (1992).
8. D. H. Rothman and S. Zaleski, Lattice-gas models of phase separation: Interfaces, phase transitions, and multiphase flow, *Rev. Mod. Phys.* **66**:1417–1479 (1994).
9. J. Olson and D. H. Rothman, Three dimensional immiscible lattice-gas: Application to sheared phase separation, *J. Stat. Phys.* **81**:199–222 (1995).
10. D. H Rothman and J. M. Keller, Immiscible cellular-automaton fluids, *J. Stat. Phys.* **52**:1119–1127 (1988).
11. A. K. Gunstensen, D. H. Rothman, S. Zaleski, and G. Zanetti, Lattice Boltzmann model of immiscible fluids, *Phys. Rev. A* **43**(8):4320–4327 (1991).
12. F. J. Alexander, S. Chen, and D. W. Grunau, Hydrodynamic spinodal decomposition: Growth kinetics and scaling functions, *Phys. Rev. B* **48**:R634 (1993).

13. S. Chen and T. Lookman, Growth kinetics in multicomponent fluids, *Phys. Rev. Lett.*, submitted (1994).
14. D. d'Humières, P. Lallemand, and U. Frisch, Lattice gas models for 3D hydrodynamics, *Europhys. Lett.* **2**:291–297 (1986).
15. C. Adler, D. d'Humières, and D. H. Rothman, Surface tension and interface fluctuations in immiscible lattice gases, *J. Phys. I France* **4**:29-46 (1994).
16. H. Furukawa, Dynamic scaling assumption for phase separation, *Adv. Phys.* **34**:703 (1985).
17. H. Tomita, Sum rules for small angle scattering by random interface, *Prog. Theor. Phys.* **72**:656 (1984).
18. H. Tomita, Statistical properties of random interface systems, *Prog. Theor. Phys.* **75**:482 (1986).
19. T. Koga and K. Kawasaki, Spinodal decomposition in binary fluids: Effects of hydrodynamic interactions, *Phys. Rev. A* **44**:R817 (1991).
20. K. Kubota, N. Kuwahara, H. Eda, and M. Sakazume, Spinodal decomposition in a critical isobutyric acid and water mixture, *Phys. Rev. A* **45**:R3377 (1992).
21. C. Yeung, Scaling and the small-wave-vector limit of the form factor in phase-ordering dynamics, *Phys. Rev. Lett.* **61**:1135–1138 (1988).
22. H. Furukawa, Multi-time scaling for phase separation, *J. Phys. Soc. Jpn.* **58**:216 (1989).
23. I. M. Lifshitz and V. V. Slyozov, The kinetics of precipitation from supersaturated solid solutions, *J. Phys. Chem. Solids* **19**:35–50 (1961).
24. E. D. Siggia, Late stages of spinodal decomposition in binary mixtures, *J. Phys. Rev. A* **20**:595–605 (1970).